Available online at www.sciencedirect.com
ScienceDirect
Journal of Nuclear Materials 366 (2007) 28–36
journal of nuclear materials
www.elsevier.com/locate/jnucmat

Effect of trace impurities in helium on the creep behavior of Alloy 617 for very high temperature reactor applications

P.S. Shankar, K. Natesan *

Argonne National Laboratory, 9700 South Cass Avenue, Argonne, IL 60439, USA

Received 7 August 2006; accepted 5 December 2006

Abstract

The effect of trace impurities, methane and oxygen, in helium on the creep behavior of Alloy 617, has been investigated. The creep rupture life at relatively low applied stresses was shortest in a helium environment containing 500 vppm oxygen ($He + O_2$), while it was the longest in helium containing 675 vppm methane ($He + CH_4$). However, the rupture strain was significantly lower in the $He + CH_4$ environment compared to that in pure helium (He) and $He + O_2$. The low rupture strain in the $He + CH_4$ is caused by cleavage fracture. In the $He + CH_4$ environment, the fracture mode was cleavage at lower applied stresses and ductile at higher applied stresses while in the He and $He + O_2$, a ductile fracture was observed at all stress levels. The apparent activation energy for creep was determined in all three environments, and it appears to be independent of stress in the He, dependent in the $He + CH_4$, while in the $He + O_2$ environment the stress dependence could not be conclusively established.

PACS: 62.20.Hg

1. Introduction

The very high temperature reactor (VHTR) is one of six nuclear reactor concepts selected by the Generation IV International Forum [1]. The United States Department of Energy is actively pursuing research on the VHTR concept for the development of next generation nuclear reactors not only due to its near-term deployment potential but also because the high temperatures generated by the VHTR can enable hydrogen production [1]. The VHTR concept is based on a modular high-temperature gas-cooled reactor concept with helium as the coolant and a closed-cycle gas turbine for power generation [2,3], in contrast to the steam-based turbines envisaged during the 1970s and 1980s. In the VHTR concept, the helium from the reactor core is used to drive the turbine directly or indirectly by heating air or nitrogen that drives the turbines. The reactor core outlet temperature/turbine inlet temperature would be ≈850 °C. Under these conditions, the primary helium coolant is expected to reach temperatures of 850–950 °C. Thus, the structural materials to be used in the VHTR concept, especially in the core, heat exchangers, and turbine sections, should

* Corresponding author. Tel.: +1 630 252 5103/5111; fax: +1 630 252 3604.
E-mail addresses: shankar@anl.gov (P.S. Shankar), natesan@anl.gov (K. Natesan).

0022-3115/$ - see front matter © 2006 Published by Elsevier B.V.
doi:10.1016/j.jnucmat.2006.12.028

possess adequate mechanical performance up to about 1000 °C in helium environments.

Gaseous helium by itself is inert, having little impact on the corrosion and mechanical properties of reactor materials. However, the helium coolant in the VHTR is expected to contain small amounts (of the order of ppm) of contaminants such as H_2, H_2O, CH_4, O_2, and CO_2. The contamination of the helium coolant can occur due to degassing, water/oil leaks, etc. Experience has shown that these contaminants cannot be completely eliminated with the purification methods currently available [4]. Past studies [4–11] have shown that these contaminants can significantly corrode the metallic materials at high temperatures, thereby affecting critical long-term mechanical properties like creep.

The corrosion of reactor structural materials (e.g., austenitic stainless steels and iron- and nickel-based superalloys) at high temperatures may involve oxidation, carburization, and/or decarburization depending on temperature, oxygen potential, and carbon activity in the gas phase. Therefore, there is a need to evaluate and develop metallic materials having improved creep resistance in helium environments containing the aforementioned impurities.

Alloy 617 is a prime candidate for VHTR structural components like reactor internals, piping, and heat exchangers [2]. Alloy 617 is a nickel-based superalloy having exceptional creep strength above 800 °C. This alloy contains Co, Mo, Al, and Ti in addition to Cr [2]. Al and Cr provide the oxidation resistance, while Co and Mo provide the solid solution strengthening. Due to the excellent mechanical properties, oxidation and creep resistance, and phase stability at high temperatures, this alloy is considered the workhorse of structural materials for use in VHTRs. There is a considerable body of work in literature [8,9,11–18] on the creep rupture properties of Alloy 617 in a helium environment for reactor applications, but all of these studies are aimed at steam-cycle and process-nuclear-heat based gas-cooled reactors. With the current thrust shifting toward development of high temperature gas-cooled reactors with a gas turbine, the creep response of these alloys needs to be re-evaluated because the level of impurities in helium is different in the steam-cycle and gas-turbine high temperature gas cooled reactors [2,6]. For example, the oxygen potential is expected to be lower in the gas turbine concept as compared to the steam generating systems. Therefore, the objective of the present study was to evaluate the uniaxial creep behavior of Alloy 617 in helium environments with various amounts of impurities. It should be mentioned that discussion of the effects of radiation on mechanical properties of Alloy 617 is outside the scope of this paper. Radiation may affect mechanical properties of structural components depending on the specific VHTR design and the radiation levels expected therein. These effects, if any, would be applicable to in-core components and reactor internals rather than on components, such as heat exchangers and piping, which will be outside the reactor away from the radiation environment.

2. Experimental

The creep behavior of Alloy 617, whose composition is given in Table 1, was evaluated at 843 and 950 °C at 1 atm in three helium environments: pure helium (He), helium with 675 vppm methane (hereafter referred to as $He + CH_4$), and helium with 500 vppm oxygen (hereafter referred to as $He + O_2$). The nominal composition of the pure helium was He-99.999%, O_2 <1 ppm, H_2O <2 ppm, and total hydrocarbons <1 ppm. A helium test facility consisting of a mass spectrometer and a micro gas chromatograph was built to control the impurity levels of methane and oxygen that simulate the helium environment in a high temperature helium-cooled reactor. The spectrometer and the chromatograph were calibrated for continuous measurement of gas phase impurities in helium. Care was taken to ensure that the impurity levels were controlled and maintained at required ppm levels throughout the tests.

Creep tests were performed according to ASTM E139-96 on polished cylindrical specimens with a gage length of 19.1 mm and a gage diameter of 3.8 mm using direct-load creep machines. The specimens were loaded at constant rate to full load at the test temperature. Creep strain in the specimens was measured by a linear variable differential transducer (LVDT) whose sensitivity is 5 μm. The LVDT was calibrated before each test to ensure consistency in strain measurements. The creep strain was continuously recorded by a data acquisition system

Table 1
Elemental composition (wt%) of Alloy 617

C	Cr	Mn	Si	Mo	Al	Fe	Ti	Co	Ni
0.08	21.6	0.1	0.1	9.5	1.2	0.9	0.3	12.5	Bal

attached to the test system. After specimen failure, creep curves were generated using the acquired creep strain and time data. Subsequently, minimum creep rate, $\dot{\varepsilon}$, was extracted from the experimental creep curves by a linear least squares analysis. Microscopic observations were performed on failed specimens to characterize the creep fracture morphology.

The aim of the creep tests was to evaluate the influence of the trace impurities in helium on the creep rupture life, rupture strain, minimum creep rate, and associated creep fracture modes. The effect of impurity content in He on the stress and temperature dependence was also evaluated.

3. Results and discussion

3.1. Uniaxial creep response

Fig. 1 shows the creep strain vs. rupture life curves in the pure He environment at 950 °C at different applied stresses. The effect of applied stress on rupture life at a given temperature is evident from these curves. At 27.6 MPa, not only the rupture life but also the rupture strain is quite high. The creep rupture behavior in pure He observed in the present study is compared with numerous previous studies [8,13,15,17,18] as shown in Fig. 2, which shows the variation of rupture life with applied stress. All the data above the dotted line in the figure had a test temperature of 843–850 °C, while those below the dotted line were tested at 950 °C. It is evident from the figure that at ≈850 °C the rupture lives observed in the present study tend to be slightly on the lower side compared to those observed by others, while at 950 °C, the rupture lives are similar in all studies except Huchtemann [8] and Schubert [13]. Schubert's [13] data (indicated by + in the figure) were obtained at an applied stress of 23 MPa (in contrast to 27.6 MPa in the present study), which might explain the higher rupture life in his study. On the other hand, the rupture life observed by Huchtemann [8] at ≈27 MPa is almost an order of magnitude lower than the present results. Huchtemann [8] attributed this degradation in rupture life to the absence of a protective oxide layer coupled with a decarburized zone.

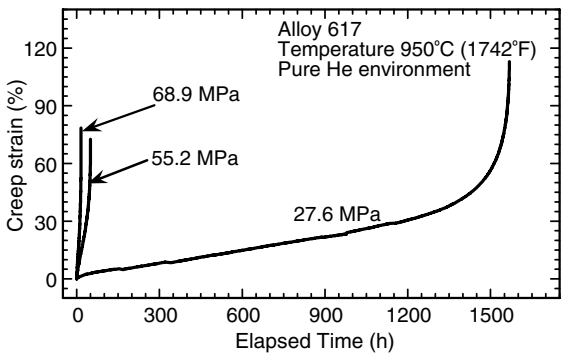

Fig. 1. Creep strain vs. time for Alloy 617 at 950 °C in pure helium environment.

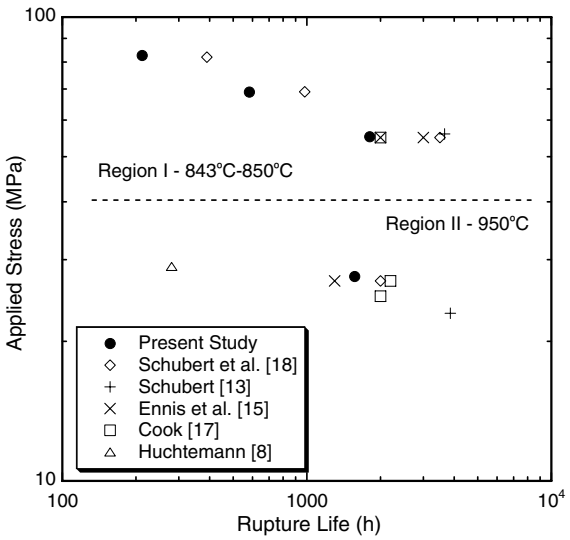

Fig. 2. Creep behavior of Alloy 617 in pure helium environment at 843–950 °C.

Figs. 3(a) and (b) show the effect of methane and oxygen impurities in helium on the creep behavior of Alloy 617 at 843 and 950 °C, respectively. The curves indicate that the rupture life is longest in the $He + CH_4$ and shortest in the $He + O_2$. The reduction in life in the $He + O_2$ environment and increase in life in the $He + CH_4$ environment is very significant at 950 °C than at 843 °C. Reduction in rupture life in an environment containing helium with 500 ppm O_2 compared to pure helium (99.995% purity) was also observed by Hosoi and Abe [11] in tests at 1000 °C. They attributed this reduction (more than 50%) to the occurrence of a decarburized zone ≈1 mm from the surface. They also observed that the maximum reduction in life occurred at 500 ppm O_2; at higher and lower O_2 levels the rupture life increased but was still lower than those observed in pure helium. The presence or absence of decarburization in our specimens tested in $He + O_2$ has not yet been characterized. The longer life in $He + CH_4$ is accompanied by a significant decrease in rupture strain when

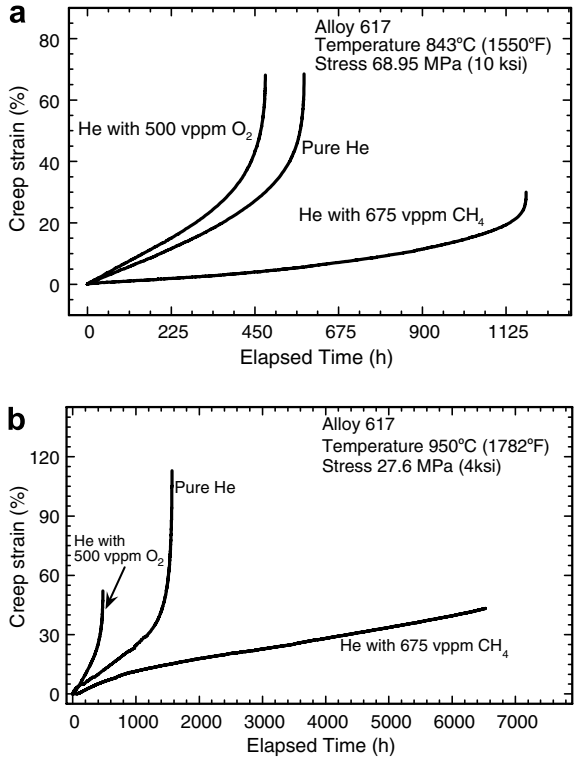

Fig. 3. Effect of methane and oxygen impurities in helium on the creep rupture behavior of Alloy 617. (a) Creep rupture behavior at 843 °C and 68.95 MPa, (b) creep rupture behavior at 950 °C and 27.6 MPa.

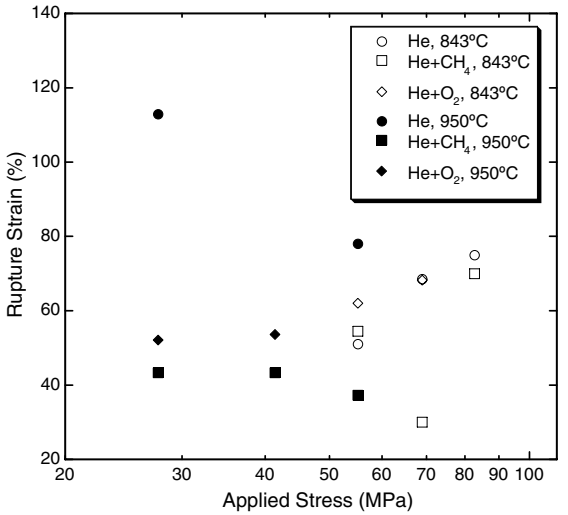

Fig. 4. Variation of rupture strain with applied stress in different helium environments.

compared to the rupture strains observed in He and $He + O_2$. Fig. 4 shows the variation of rupture strain versus applied stress in all three environments used in the current study. The data show a degrading effect of methane on rupture strain at both test temperatures. A decrease in rupture elongation in pure helium environment when compared to air has been observed previously [17,18]. Table 2 presents creep data for Alloy 617 at 843 °C and 950 °C in He, $He + CH_4$, and $He + O_2$ obtained from the present study. At 950 °C and 27.6 MPa in $He + CH_4$, the specimen had accumulated >6500 h and the creep curve seemed to indicate sufficient ductility (≈40%) during the test period. However, upon termination of the test and cooling the specimen to room temperature, the specimen fractured (literally split into two pieces) indicating brittle behavior of the alloy due to exposure.

3.2. Temperature and stress dependence of creep

In as much as creep involves a thermally activated process, the minimum creep rate, $\dot{\varepsilon}$, can be expressed [19,20] as

$$\dot{\varepsilon} = A\sigma^n \exp\left(\frac{-Q}{RT}\right), \tag{1}$$

where σ is the applied stress, n is the stress exponent, Q is the apparent activation energy for creep mechanism, A is a constant, R is the universal gas constant, and T is the absolute temperature. Using the creep rates derived from experimental data, a multiple linear regression analysis was performed as a function of $\ln\sigma$ and $1/T$ to estimate n and Q in all three environments. The calculated values of n and Q, given in Table 3, suggest a 5th-power relationship [19,21] between stress and creep rate for He and $He + CH_4$ and a 3rd-power relationship for $He + O_2$. Stress exponent ≈5 indicates dislocation climb- and/or glide-controlled creep [19,21], whereas $n \approx 3$ suggests a viscous glide mechanism [22] as the rate-controlling step.

Provided there is a weak dependence of activation energy on stress, the stress dependence of creep can be approximated from Norton's relationship [23],

$$\dot{\varepsilon} = A\sigma^n. \tag{2}$$

Usually, most metallic materials in the stress range $10^{-4} < \sigma/E < 10^{-2}$ follow Eq. (2) with $n \approx 5$ [24]. The minimum creep rate vs. stress is plotted in Fig. 5. The figure also shows the values of the stress exponent, n calculated from the slope of the best-fit straight lines. As shown in the figure, in pure He, the

Table 2
Creep rupture data of Alloy 617 at 843 °C and 950 °C in different helium environments

Environment	Temperature (°C)	Applied stress (MPa)	Rupture life (h)	Rupture strain (%)	Minimum creep rate (s^{-1})
Pure He	843	55.2	1807	51.00	3.8×10^{-8}
		68.95	582	68.50	1.5×10^{-7}
		82.7	204	74.70	4.6×10^{-7}
He with 675 vppm methane	843	55.2	1668	51.42	4.8×10^{-8}
		68.95	1179	30.04	2.5×10^{-8}
		82.7	191	69.95	4.5×10^{-7}
He with 500 vppm oxygen	843	55.2	1223	62.00	6.9×10^{-8}
		68.95	478	68.25	1.9×10^{-7}
Pure He	950	27.6	1568	112.90	6.6×10^{-8}
		55.2	50	72.58	2.1×10^{-6}
		68.95	16	78.44	6.6×10^{-6}
He with 675 vppm methane	950	27.6	>6527[a]	43.30	1.5×10^{-8}
		41.4	587	43.30	1.3×10^{-7}
		55.2	81	37.30	4.9×10^{-7}
He with 500 vppm oxygen	950	27.6	475	52.10	1.6×10^{-7}
		41.4	184	53.60	4.2×10^{-7}

[a] Test terminated and specimen cooled to room temperature.

Table 3
Values of n and Q calculated by multiple regression analysis

Environment	Stress exponent, n	Activation energy, Q (kJ/mol)
Pure helium	5.2	408
He + CH_4	5.09	309
He + O_2	2.88	270

n values obtained at both 843 °C and 950 °C suggest a 5th-power creep mechanism [24]. These n values are roughly the same as the n value in Table 3, estimated by the multiple regression analysis using Eq. (1). The similar n values suggest that Eq. (2) provides a good approximation for the stress dependence of creep at a given temperature in pure He. In other words, one can infer weak dependence of activation energy on stress in pure He in the temperature range investigated. This inference was also confirmed by calculating Q at 55.2 MPa and 68.95 MPa using the following equation [25]:

$$Q = \frac{R\left(\ln\frac{\dot{\varepsilon}_1}{\dot{\varepsilon}_2}\right)}{\left(\frac{1}{T_2}-\frac{1}{T_1}\right)}. \quad (3)$$

The calculated Q values were 425 kJ/mol at 55.2 MPa and 401 kJ/mol at 68.95 MPa, in close agreement with the Q value in Table 3. Eq. (3) assumes that the same creep mechanism operates at both T_1 and T_2 temperatures. The use of Eq. (3) to calculate Q is justified because 5th-power creep behavior is followed at both 843 °C and 950 °C in He.

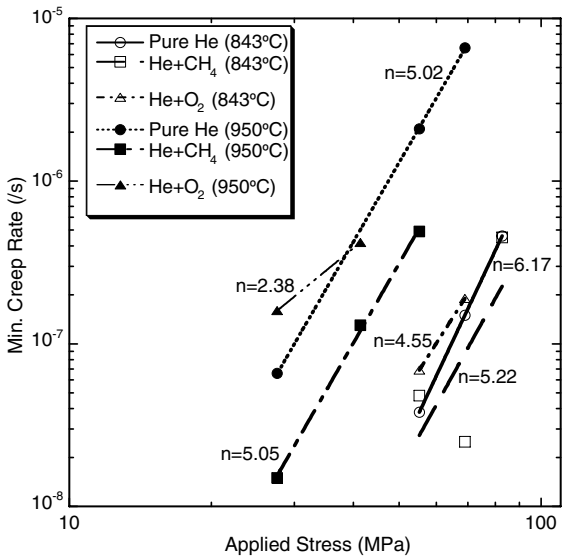

Fig. 5. Stress dependence of minimum creep rate of Alloy 617 at 843 °C and 950 °C in He, He + CH_4, and He + O_2 environments. Values of the stress exponent, n are also shown in the figure.

In the case of He + CH_4, the stress exponent shown in Table 3 is similar to the values ($n = 5.22$ at 843 °C and $n = 5.05$ at 950 °C) in Fig. 5. However, as can be seen in Fig. 5, the best-fit straight line for He + CH_4 at 843 °C (with $n = 5.22$) does not

connect all the corresponding experimental data points. This may be due to a different creep fracture mechanism at different stresses. Furthermore, the apparent activation energy calculated using Eq. (3) is 246 kJ/mol at 55.2 MPa (reasonably close to that estimated by regression analysis), whereas it is 439 kJ/mol at 68.95 MPa (much higher than the value in Table 3). Thus, the apparent activation energy appears to depend on stress in $He + CH_4$ in the temperature range studied.

In $He + O_2$, the n values in Fig. 5 are very different at the two test temperatures: $n = 2.38$ at 950 °C, close to the value obtained in Table 3, and $n = 4.55$ at 843 °C. This difference suggests a possible dependence of activation energy on stress in $He + O_2$. In addition, the n values at these two temperatures indicate a different creep mechanism (viscous glide at $n = 2.38$ and dislocation creep at $n = 4.55$), which precludes the use of Eq. (3) to calculate Q. More experiments are needed at different stresses at these two temperatures to confirm the presence (or absence) of stress dependence of activation energy.

The apparent activation energy for creep in the pure He environment from Table 3 is 408 kJ/mol. For a 5th-power creep mechanism, as observed in pure He, the activation energy for creep is expected to be equal to the activation energy for lattice self-diffusion, Q_{sd} [19,21]. The Q determined in the present study (408 kJ/mol) is higher than the Q_{sd} of nickel (≈285 kJ/mol) [25]. Higher apparent activation energy than Q_{sd} has been observed in nickel solid solution alloys exhibiting $n \approx 5$ and can be expected when the temperature dependence of elastic modulus and effect of friction stress are not considered [26,27]. The apparent activation energies in the $He + CH_4$ and $He + O_2$ environments are 309 kJ/mol and 270 kJ/mol, respectively, as determined by multiple regression analysis. These Q values are comparable to the activation energy for self-diffusion of nickel and suggest a 5th-power dislocation creep mechanism. However, as mentioned earlier, the actual creep mechanism in these two environments may be 5th-power-law creep, or a 3rd-power-law creep, or a combination of these that could change the actual activation energies mentioned above.

3.3. Failure modes in creep

Figs. 6(a)–(c) show the fracture surface of ruptured specimens after exposure to 27.6 MPa at 950 °C in He, $He + O_2$, and $He + CH_4$, respectively. A transgranular ductile fracture is observed in He and $He + O_2$, as evident in Fig. 6(a) and (b), respectively. In pure He (Fig. 6(a)), there also appears to be a relatively larger proportion of voids compared to $He + O_2$. Hosoi and Abe's work on creep of

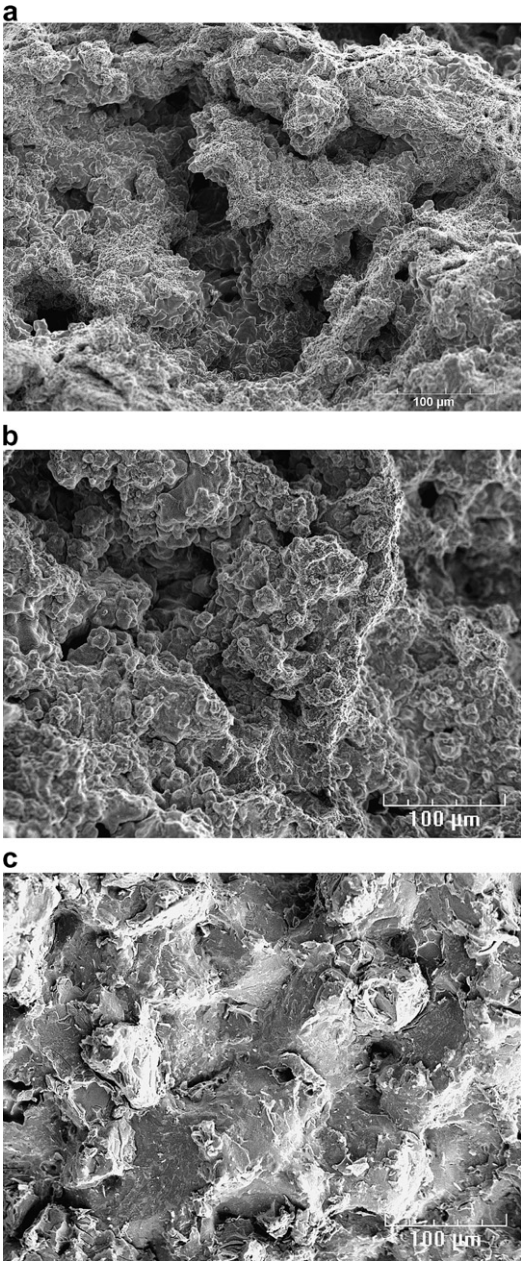

Fig. 6. Creep fracture modes of Alloy 617 at 950 °C and 27.6 MPa in different helium environments. (a) Ductile fracture in pure He, (b) ductile fracture in $He + O_2$, (c) cleavage fracture in $He + CH_4$.

Alloy 617 did not address the fracture modes observed in He and He + O_2, and this omission prevents a direct comparison of our observations with theirs [11]. Fig. 6(c) shows that the fracture surface in the specimen creep tested in He + CH_4 exhibits a faceted morphology, which indicates a cleavage mode of fracture. Evidence of secondary cracking at facet/grain boundaries can also be seen in Fig. 6(c). Furthermore, the entire fracture surface area of the specimen shown in Fig. 6(c) exhibited a blocky intergranular-type faceted fracture morphology. The fracture mode in the specimen creep tested in He + CH_4 (at both temperatures) at lower applied stresses can be characterized as mixed intergranular/transgranular cleavage. In specimens tested at 843 °C and at lower applied stresses, although the fracture morphologies were slightly different from those observed at 950 °C, similar fracture modes were observed in all three environments, i.e., ductile in He and He + O_2 and cleavage in He + CH_4. None of the previous creep studies [8,11,12,15], except a report by McCoy and King [28], on Alloy 617 in helium environments noted the occurrence of cleavage fracture, either because there were no tests performed with controlled addition of methane to helium as done in the present study or maybe cleavage fracture does not occur in the high-oxygen-potential helium environments that were used in those studies. McCoy and King [28] observed intergranular cleavage fracture of Alloy 617 at 593 °C and 871 °C in an impure helium environment containing 337 ppm H_2, 32 ppm CH_4, 19 ppm CO, 2 ppm H_2O and <0.5 ppm N_2. The substantial reduction of rupture strain observed (Fig. 3(a) and (b)) at lower applied stresses in the specimens tested in He + CH_4 compared to those tested in He and He + O_2 can be attributed to the occurrence of cleavage fracture. At higher applied stresses, evidence of cleavage fracture was not seen in He + CH_4. The fracture mode was ductile in all three environments.

Fig. 7 shows a longitudinal cross-section of the fracture surface of the specimen shown in Fig. 6(c) that was creep tested in He + CH_4 environment. The dark phase in the figure was identified as chromium carbide ($Cr_{23}C_6$), and the brighter phase is an intermetallic phase of chromium and molybdenum. The figure shows a coarse $Cr_{23}C_6$ network with clear indication of preferential crack propagation along the carbide phase. The Cr–Mo intermetallic phase may also crack with exposure time due to its inherent brittleness. The alloy's propensity to crack along

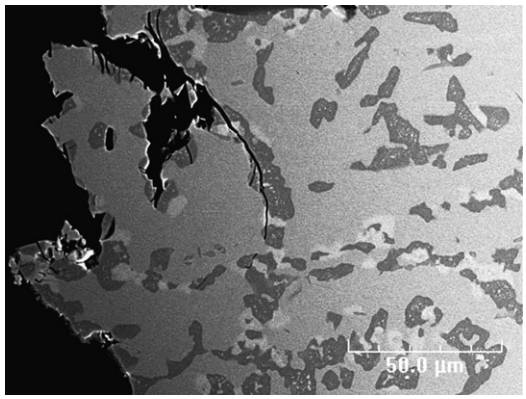

Fig. 7. Longitudinal section of specimen in Fig. 6(c) indicating crack propagation along coarse $Cr_{23}C_6$ phase.

the carbide and/or intermetallic phase may, under creep-fatigue operating conditions in a VHTR, lead to rapid crack initiation and propagation, which could severely decrease the operating life of reactor components made of this alloy. Microstructural analysis of longitudinal cross-sections of fracture surfaces of specimens creep tested in He and He + O_2 did not show clear evidence of coarse chromium carbide precipitation. The precipitation of grain boundary carbides of the type $M_{23}C_6$ and M_6C (M = metal) has been shown to pin grain boundary migration, leading to higher creep strength in Alloy 617 and other nickel alloys [27,29,30]. Furthermore, studies have also indicated that once the $M_{23}C_6$ carbides coarsen, grain boundary migration occurs leading to creep deformation [15,17]. A recent study has also suggested that under conditions of carburization, these carbides can embrittle the alloy, leading to lower creep ductility [31]. A similar reasoning, i.e., grain boundary pinning by carbides and embrittlement by carbide coarsening, may be a possible explanation for the increased creep rupture life and reduced rupture strain in He + CH_4 than in He and He + O_2. Clearly, additional studies are needed to validate this line of reasoning.

Based on the microstructural and fractographic observations described above, it appears that an interplay of two factors is required for cleavage fracture under creep loading:

(a) Lower applied stresses that, by themselves, are not enough to overcome the required barriers for deformation. Under such low stresses, the environmental species (CO, H_2, etc.) in helium

gas have enough time to diffuse to preferential areas (e.g., H_2 at grain boundaries) and/or to react completely with the alloying elements to form phases, like coarse $Cr_{23}C_6$, that could initiate cleavage cracking [25,27,31]. The fact that cleavage fracture did not occur at higher applied stresses indicates that environmental effects were not significant enough to cause cleavage fracture. Generally, higher applied stresses can by themselves overcome the deformation barriers, thereby precluding time-dependent processes, like gaseous diffusion and corrosion, to significantly affect deformation behavior.

(b) A favorable combination of environment, temperature, and gas chemistry to form an extensive distribution of coarse $Cr_{23}C_6$, which could initiate cleavage cracking [31]. Even at lower applied stresses, where the effects of environmental species can be considerable, the He and He + O_2 specimens did not exhibit cleavage fracture, suggesting that favorable environmental conditions were not present for coarse $Cr_{23}C_6$ precipitation.

Both the above factors (lower applied stress and a favorable chemistry and environment) seem to be required to act together to cause cleavage. In addition, micromechanisms that are unknown at this time may be operating. A detailed microstructural analysis to investigate the extent of carburization, decarburization, and/or oxidation and the nature of scaling and internal phase formation is in progress to understand the nature of corrosion/oxidation occurring in the different environments and its effect on the macroscopic creep response.

4. Summary

A preliminary investigation was conducted to evaluate the effect of controlled amounts of impurities (methane and oxygen) in gaseous helium on the creep response of Alloy 617 at 843 °C and 950 °C. A helium test facility was set-up that ensured accurate control of the impurities at the required level during the creep tests.

Alloy 617 in He + CH_4 environment shows the lowest rupture strain and longest life at lower applied stresses while in the He + O_2 environment, the alloy exhibits the shortest life. The reduction in creep rupture strain in He + CH_4 is attributed to the occurrence of cleavage fracture.

In the pure helium environment, the alloy exhibits dislocation climb-controlled creep behavior with a stress exponent of $n \approx 5$. The apparent activation energy for creep, $Q = 408$ kJ/mol, was found to be independent of stress in the pure He environment. In He + CH_4, the multiple regression analysis suggested dislocation climb-controlled creep behavior ($n \approx 5$) with an apparent activation energy for creep, $Q = 309$ kJ/mol. However, analysis using Norton's law suggested that $n \approx 5$ at 950 °C, and that n could vary with stress at 843 °C. The apparent activation energy for creep is believed to be stress dependent in the He + CH_4 environment. In He + O_2, the multiple regression analysis indicated a viscous glide mechanism for creep with $n \approx 3$, while Norton's equation suggested $n \approx 3$ at 950 °C and $n \approx 5$ at 843 °C. The apparent activation energy for creep was determined to be 270 kJ/mol. The stress dependence of activation energy in the He + O_2 environment could not be conclusively established.

Creep fracture in He and He + O_2 environments occurs by a ductile mode at all stress levels. In He + CH_4, the fracture mode was cleavage at lower applied stresses and ductile at higher applied stresses. It is believed that lower applied stresses and a favorable environmental condition are required to form a coarse network of $Cr_{23}C_6$ phase that appears to initiate cleavage cracking. The different fracture behavior/modes in different environments and stresses clearly suggest a complex interaction of the environment, stress, and temperature with the alloying elements in the VHTR operating conditions. The impurities in the helium gas need to be tailored such that the $Cr_{23}C_6$ phase provides an optimum level of grain boundary pinning (to increase creep strength) without compromising ductility. The results of this ongoing study indicate a critical need to establish the performance envelope for candidate materials for use in heat exchangers and other components in VHTRs and to specify the purity requirements for the reactor helium for acceptable long-term performance of materials in VHTRs.

Acknowledgments

This work was initiated under the sponsorship of the US Nuclear Regulatory Commission and continued under US Department of Energy contract W-31-109-Eng-38.

References

[1] A Technology Roadmap for Generation IV Nuclear Energy Systems, US DOE Nuclear Energy Research Advisory Committee and the Generation IV International Forum, December 2002.
[2] K. Natesan, A. Purohit, S.W. Tam, NUREG/CR-6824/ANL-02/37, 2003.
[3] R. Couturier, C. Escaravage, in: IAEA-TECDOC-1238, IAEA Technical Committee Meeting on Gas Turbine Power Conversion Systems for Modular HTGRs, 2000, p. 161.
[4] M. Cappelaere, M. Perrot, J. Sannier, Nucl. Technol. 66 (1984) 465.
[5] W.R. Johnson, G.Y. Lai, Report IWGGCR-4, IAEA Specialists Meeting on High Temperature Metallic Materials for Application in Gas-Cooled Reactors, Paper J1, 1981.
[6] L.W. Graham, K.G.E. Brenner, K. Krompholz, Report IWGGCR-4, IAEA Specialists Meeting on High Temperature Metallic Materials for Application in Gas-Cooled Reactors, Paper K1, 1981.
[7] L.W. Graham, J. Nucl. Mater. 171 (1990) 76.
[8] B. Huchtemann, Mater. Sci. Eng. A 121 (1989) 623.
[9] H.M. Yun, P.J. Ennis, H. Nickel, H. Schuster, J. Nucl. Mater. 125 (1984) 258.
[10] W.J. Quadakkers, Mater. Sci. Eng. 87 (1987) 107.
[11] Y. Hosoi, S. Abe, Metall. Trans. 6A (1975) 1171.
[12] F. Schubert, U. Bruch, R. Cook, H. Diehl, P.J. Ennis, W. Jakobeit, H.J. Penkalla, E.T. Heesen, G. Ullrich, Nucl. Technol. 66 (1984) 227.
[13] F. Schubert, in: IWGGCR-9, Specialists' Meeting on Heat Exchanging Components of Gas-Cooled Reactors, 1984, p. 309.
[14] T. Tanabe, Y. Sakai, T. Shikama, M. Fujitsuka, H. Yoshida, R. Watanabe, Nucl. Technol. 66 (1984) 260.
[15] P.J. Ennis, K.P. Mohr, H. Schuster, Nucl. Technol. 66 (1984) 363.
[16] K. Schneider, W. Hartnagel, P. Schepp, B. Ilschner, Nucl. Technol. 66 (1984) 289.
[17] R.H. Cook, Nucl. Technol. 66 (1984) 283.
[18] F. Schubert, H.J. Seehafer, E. Bodmann, J. Eng. Power 105 (1983) 713.
[19] O.D. Sherby, P.M. Burke, Prog. Mater. Sci. 13 (1967) 325.
[20] K. Natesan, W.K. Soppet, A. Purohit, J. Nucl. Mater. 307–311 (2002) 585.
[21] M.E. Kassner, M.T. Perez-Prado, Prog. Mater. Sci. 45 (2000) 1.
[22] B. Wilshire, R.W. Evans (Eds.), Creep Behavior of Crystalline Solids, Pineridge, UK, 1985.
[23] F.H. Norton, The Creep of Steel at High Temperatures, McGraw-Hill, NY, 1929, p. 124.
[24] T.G. Langdon (Ed.), Dislocations and Properties of Real Materials, Proceedings of the Conference of Institute of Metals, London, 1984, p. 221.
[25] R.W. Hertzberg, Deformation and Fracture Mechanics of Engineering Materials, 4th Ed., John Wiley, NY, 1996.
[26] J.T. Guo, C. Yuan, H.C. Yang, V. Lupinc, M. Maldini, Metall. Trans. 32A (2001) 1103.
[27] C.T. Sims, N.S. Stoloff, W.C. Hagel (Eds.), Superalloys II, Wiley, NY, 1987.
[28] H.E. McCoy, J.F. King, ORNL/TM-9337, Oak Ridge National Laboratory, 1985.
[29] S. Kihara, J.B. Newirk, A. Ohtomo, Y. Saiga, Metall. Trans. (1980) 1019.
[30] K. Mino, A. Ohtomo, Trans. Iron Steel. Inst. Jpn. 18 (1978) 731.
[31] D. Kaczzorowski, P. Combrade, in: ICONE 13-50634, Proceedings of 13th International Conference on Nuclear Engineering, Beijing, China, May 2005.